Analytica Chimica Acta 810 (2014) 71–78

Contents lists available at ScienceDirect

Analytica Chimica Acta

journal homepage: www.elsevier.com/locate/aca

Sensors and Bioselective Reagents

Fluorescent blood glucose monitor by hemin-functionalized graphene quantum dots based sensing system

Yuezhen He, Xiaoxun Wang, Jian Sun, Shoufeng Jiao, Hongqi Chen, Feng Gao, Lun Wang*

Anhui Key Laboratory of Chemo-Biosensing; Key Laboratory of Functional Molecular Solids, Ministry of Education,; College of Chemistry and Materials Science, Anhui Normal University, Wuhu 241000, People's Republic of China

HIGHLIGHTS

- Hemin is assembled onto the surfaces of graphene quantum dots (GQDs).
- With the aid of hemin, H_2O_2 could quench the FL signal of GQDs obviously.
- Based on this effect, a fluorescent platform is proposed for the sensing of glucose.
- The proposed method provides a new pathway to explore practical application of GQDs.

GRAPHICAL ABSTRACT

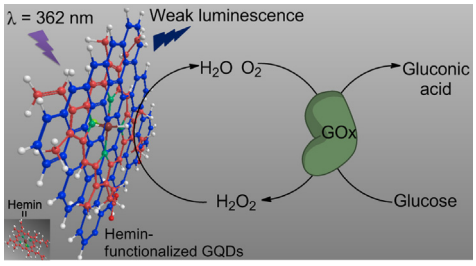

ARTICLE INFO

Article history:
Received 11 June 2013
Received in revised form
29 November 2013
Accepted 30 November 2013
Available online 7 December 2013

Keywords:
Graphene quantum dots
Hemin
Hydrogen peroxide
Glucose
Glucose oxidase
Biosensor

ABSTRACT

In the present work, a highly sensitive and specific fluorescent biosensor for blood glucose monitoring is developed based on hemin-functionalized graphene quantum dots (GQDs) and glucose oxidase (GOx) system. The GQDs which are simply prepared by pyrolyzing citric acid exhibit strong fluorescence and good water-solubility. Due to the noncovalent assembly between hemin and GQDs, the addition of hemin can make hydrogen peroxide (H_2O_2) to destroy the passivated surface of GQDs, leading to significant fluorescence quenching of GQDs. Based on this effect, a novel fluorescent platform is proposed for the sensing of glucose. Under the optimized conditions, the linear range of glucose is from 9 to 300 μM, and the limit of detection is 0.1 μM. As unique properties of GQDs, the proposed biosensor is green, simple, cost-efficient, and it is successfully applied to the determination of glucose in human serum. In addition, the proposed method provides a new pathway to further design the biosensors based on the assembly of GQDs with hemin for detection of biomolecules.

© 2013 Elsevier B.V. All rights reserved.

1. Introduction

Semiconductor quantum dots (QDs), as photoluminescent nanomaterials, have been intensively studied in sensing and cell imaging due to their excellent performance and size-tunable optical properties [1,2]. Even with these advantages, heavy metals which are the essential elements in available high-performance semiconductor QDs have suffered from intrinsic limitations such as potential toxicity and environmental hazards [3,4]. Therefore, the search for benign alternative has become increasingly important and urgent. Recently, graphene quantum dots (GQDs) as an exciting class of carbon nanomaterial, have emerged as potential new platform in fluorescent (FL) biosensing and imaging [5,6]. GQDs, which are graphene sheets smaller than 100 nm, exhibit bright fluorescence due to quantum confinement and edge effects [7]. In addition, GQDs have the excellent properties of high biocompatibility, low-toxicity, chemical inertness and good water-solubility [8,9]. Therefore GQDs are currently the eco-friendly alternatives to toxic metal-based QDs. However, most studies are focused on the preparation and property of GQDs,

* Corresponding author. Tel.: +86 553 5910008; fax: +86 553 5910008.
E-mail address: wanglun@mail.ahnu.edu.cn (L. Wang).

0003-2670/$ – see front matter © 2013 Elsevier B.V. All rights reserved.
http://dx.doi.org/10.1016/j.aca.2013.11.059

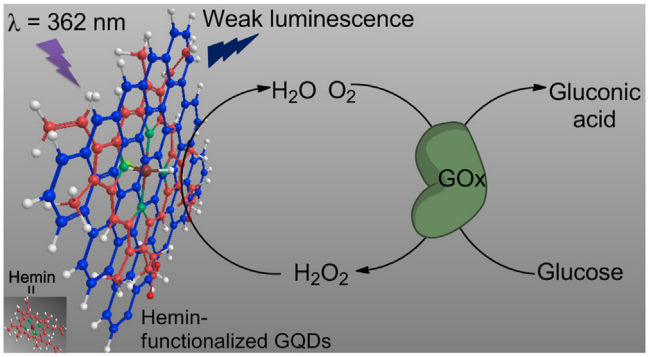

Scheme 1. Schematic illustration of the FL biosensor by hemin-functionalized GQDs.

and their analytical applications still remain at an early stage [10].

The functional modification and assembly of GQDs are essential for GQDs related applications [11]. In principle, GQDs are graphene-like smaller polycyclic aromatic hydrocarbon molecules and contain many carboxylic acid moieties at their surface, thus they can be functionalized by covalent and noncovalent interactions with various organic, inorganic, or biological species [12]. When organic molecules are covalently bound to the surface of GQDs, their extended aromatic character would be perturbed and result in the impairment of optical properties [13]. Noncovalent functionalization by π-interactions is an attractive method, because it offers the possibility of attaching functional groups without disturbing the electronic network. Hence coupling GQDs and biomolecules through π-interactions to develop high-performance sensors for biomolecular recognition is highly expected.

As a well-known natural metalloporphyrin, hemin which has intrinsic peroxidase-mimicking activity can be assembled onto the surfaces of grapheme through π–π stacking and electrostatic interactions [14–17]. Label-free colorimetric detection of single-nucleotide polymorphism has been reported based on hemin-graphene hybrid nanosheets [18]. Wu et al. constructed a label-free electrochemiluminescence sensor for telomerase detection based on porphyrin-functionalized graphene [19]. Tu et al. designed direct electrochemistry and amperometric biosensing based on picket-fence porphyrin and reduced graphene oxide through π–π interactions [20]. Song et al. reported a selective, quantitative and fast colorimetric detection of cancer cells using a folic acid conjugated graphene-hemin composite [21]. Inspired by the above reports, we designed a label-free ultrasensitive FL biosensor to detect hydrogen peroxide (H_2O_2) and glucose based on hemin-functionalized GQDs. As shown in Scheme 1, the FL sensing platform was constructed by the noncovalent assembly of hemin on GQDs through electrostatic and π–π stacking interactions. With the aid of hemin, H_2O_2 could destroy the passivated surface of GQDs and quench the FL signal obviously. As the FL quenching of hemin-functionalized GQDs was H_2O_2-concentration-dependent, a label-free, green and simple FL biosensor was established for the determination of H_2O_2 and glucose.

2. Experiment section

2.1. Materials and instruments.

Hemin and citric acid were purchased from Aladdin chemistry Co. Ltd (Shanghai, China). Hemin stock solution (5 mM) was prepared in dimethyl sulfoxide (DMSO) and stored in the dark at −20 °C. 30% H_2O_2, glucose were purchased from Shanghai Chemical Reagent Co., Ltd (Shanghai, China). Glucose oxidase was obtained from Shanghai Sagon Biotech Laboratory, Ltd (Shanghai, China). Other reagents were brought from Sinopharm Chemical Reagent Co. Ltd (Shanghai, China). All the other reagents were of analytical reagent grade and used without further purification. Doubly distilled water was used throughout the experiments.

Transmission electron micrographs (TEM) were obtained with a Tecnai G220S-TWIN transmission electron microscope (FEI).The fluorescence spectra were performed using a Hitachi F-4500 fluorescence spectrophotometer (Hitachi, Japan) equipped with a quartz cell (1 cm × 1 cm). UV–vis absorption spectra were obtained using a UV-3010 recording spectrophotometer (Hitachi, Japan). FTIR spectra were measured on a FTIR-8400S spectrometer in the 480–4000 cm^{-1} region using a powered sample on a KBr plate (Japan, Shimadzu).

2.2. Synthesis of GQDs.

The GQDs were synthesized according to the literature [22]. Briefly, 2 g of citric acid was put into a 5 mL beaker and heated to 200 °C for about 20 min, until the citric acid changed to an orange liquid. Under vigorous stirring, the obtained orange liquid was added by dropwise into 100 mL of 10 mg mL^{-1} NaOH solution. The obtained GQDs solution was adjusted to pH 7 with 10 mg mL^{-1} HCl solution. The product was subsequently purified by dialyzing through the molecular porous membrane tubing (Retained molecular weight: 1000 Da).

2.3. Procedures for FL detection of H_2O_2 and glucose

FL detection of H_2O_2: In a series of 10.0 mL volumetric flasks, 1 mL 0.5 g L^{-1} GQDs, 1.0 mL of 25 μM hemin solutions, and various amounts of H_2O_2 were added. Then the mixture was diluted to the mark with 20 mM PBS and incubated at room temperature for 10 min. The fluorescence intensity of the mixture was measured with 1 cm × 1 cm quartz cells of the F-4500 spectrofluorometer. The excitation was set at 362 nm. The slit of the excitation and emission wavelengths were set at 5 nm and the voltage was set at 400 V.

Glucose detection was tested as follows: (a) 100 μL of 20 mg mL^{-1} GOx and 8 mL of different concentrations of glucose in 20 mM PBS (pH 7.0) were incubated at 37 °C for 30 min. (b) 1.0 mL of 0.5 mg mL^{-1} GQDs and 1.0 mL of 25 μM hemin were added into the above glucose reaction solution, and incubated at room temperature for 10 min. The mixed solution was used to perform the spectroscopy measurement.

3. Result and discussion

3.1. Self-assembly of GQDs and hemin

The as-prepared GQDs aqueous solution showed bright blue emission under excitation of 362 nm UV light. The quantum yield of GQDs was calculated to be about 14% using quinine sulfate as the standard. Hemin is introduced via simple adsorption on the surface of GQDs to form hemin-GQDs hybrid nanocomposites. GQDs in aqueous dispersion are negatively charged because of their residual carboxyl groups and thus can be viewed as a 0D anionic conjugated polymer [16]. Therefore, as a positively charged 18 π-electron porphyrin, hemin molecules can be assembled onto the surfaces of GQDs to form complexes through electrostatic and π–π stacking interactions. The interplay between GQDs and hemin molecules during the process of assembly was studied by the use of UV–visible spectroscopy. As shown in Fig. 1A, GQDs exhibited an apparent UV–visible absorption band centered at 362 nm, which corresponded well to the excitation spectra. The spectrum of hemin solution contained a strong peak at 386 nm attributed to the Soret band. Upon hemin absorbed on the surface of GQDs, an absorption

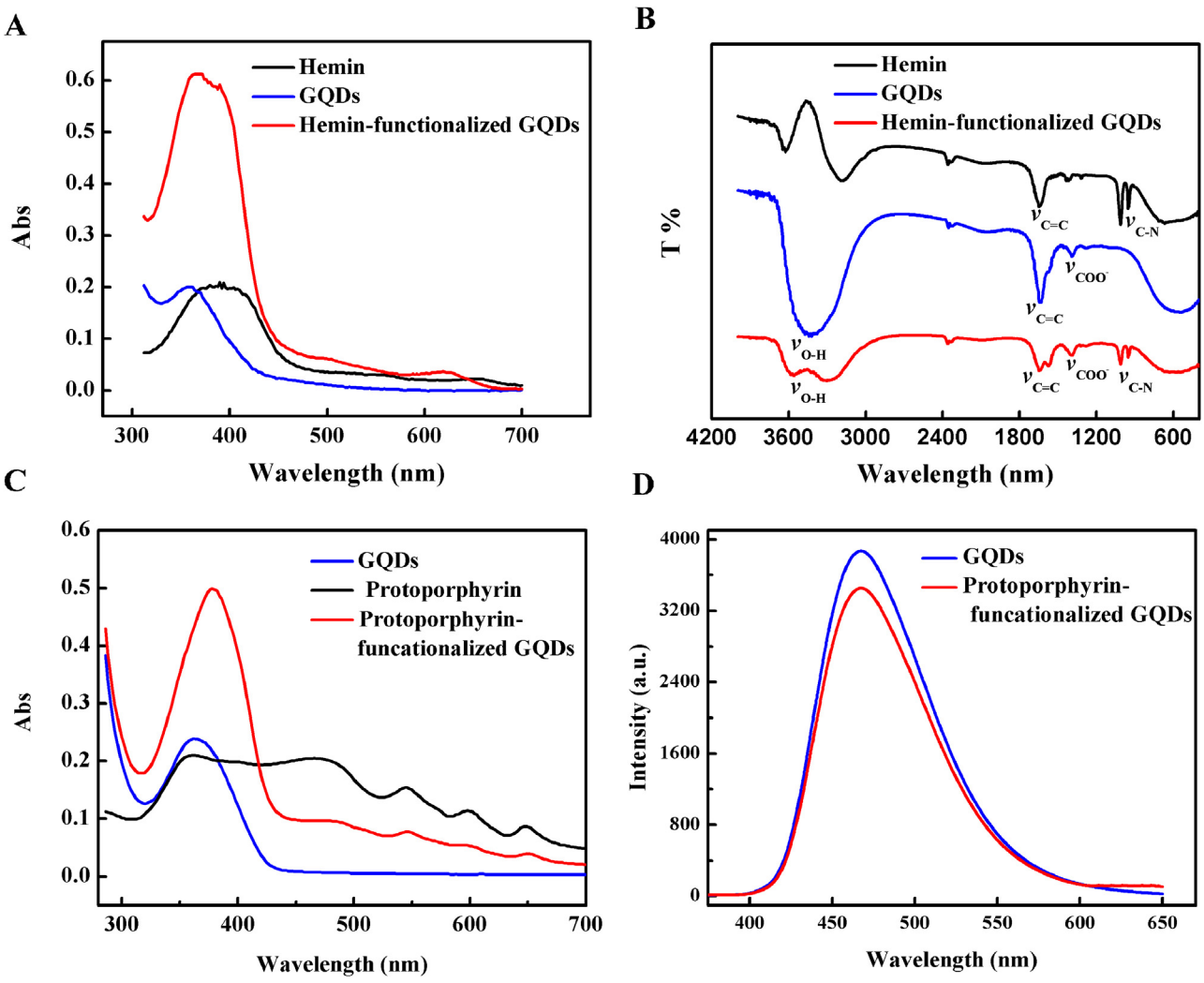

Fig. 1. (A) Absorption spectra of hemin (black line), GQDs (blue line) and hemin-functionalized GQDs (red line); (B) FTIR spectra of hemin (black line), GQDs (blue line), and hemin-functionalized GQDs (red line); (C) Absorption spectra of protoporphyrin (black line), GQDs (blue line) and protoporphyrin-functionalized GQDs (red line); (D) FL spectrum of GQDs (blue line) and protoporphyrin-functionalized GQDs (red line). (For interpretation of the references to color in this figure legend, the reader is referred to the web version of this article.)

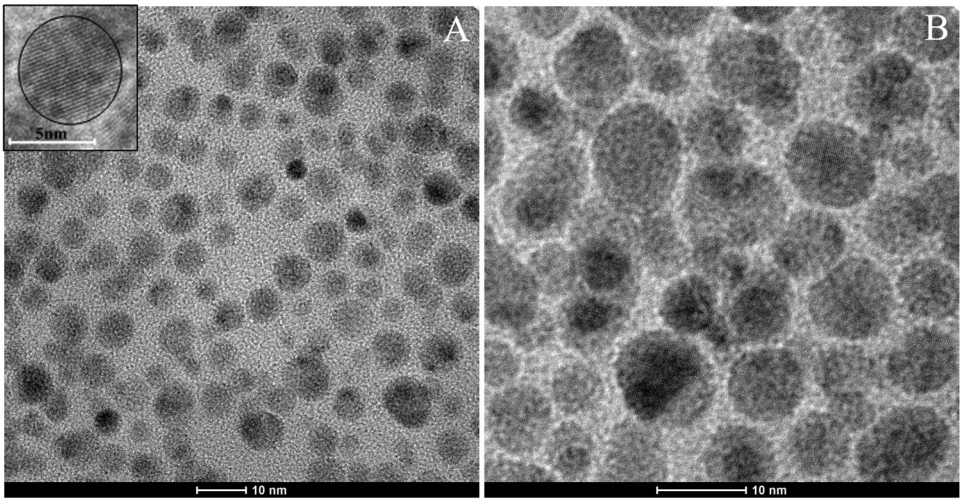

Fig. 2. (A) TEM images of GQDs, inset of (A) is the HRTEM of GQDs; (B) TEM images of hemin-functionalized GQDs;.

peak at 372 nm was enhanced. On the basis of the spectral results described above, it is reasonable to conclude that a hemin-GQDs complex was formed by simply mixing the solutions of both GQDs and hemin. However, the Soret band of hemin-functionalized GQDs didn't show a red-shift in UV absorption spectra, which could be attributed to electrostatic interaction besides π–π stacking interaction. To further confirm the molecular interaction, we tested the aqueous solution of GQDs with protoporphyrin, since protoporphyrin has a molecular structure similar to that of hemin. As protoporphyrin is an electrically neutral porphyrin, the electrostatic interactions between porphyrin and GQDs can be eliminated. The spectrum of protoporphyrin solution contained a strong peak at 360 nm attributed to the Soret band (Fig. 2C). Upon protoporphyrin absorbed on the surface of GQDs, an absorption peak at 380 nm was observed, which corresponds to the Soret band of protoporphyrin at 360 nm with a bathochromic shift (20 nm). These results indicated that protoporphyrin molecules can be assembled onto the surface of GQDs to form complexes through π–π stacking interactions. FL spectroscopy also supports this conclusion (Fig. 2D). After GQDs was mixed with protoporphyrin, an inhibition extent of about 10.2% was observed, which the reasons could be the effect of assembled protoporphyrin on the FL intensity of GQDs. Therefore, the absorption and fluorescence spectral results signify that protoporphyrin molecules can be assembled onto the surfaces of GQDs to form complexes through π–π stacking interactions. In view of the compositions and structures of hemin molecules and GQDs sheets, it can be reasonably concluded that the interactions between the two are electrostatic and π–π stacking interactions.

FTIR spectroscopy also demonstrates that hemin molecules can strongly adsorb on the surface of GQDs. As shown in Fig. 1B, the FTIR spectrum of hemin shows the stretching frequencies for C=C bond at 1647 cm^{-1} and C–N bond at 1041 cm^{-1}. The spectrum of GQDs presents intense absorption features: around 1631 cm^{-1} from C=C bond, around 3402 cm^{-1} from –OH groups and 1395 cm^{-1} from–COO^{-}. When hemin was combined with GQDs, 1631 cm^{-1} almost disappeared, and a new broad band emerges at 1573 cm^{-1}. The stretching band of the amide C–N peak appears at 1068 cm^{-1}. Overall, these results provided supportive evidence that hemin molecules could be strongly adsorbed on the GQDs' surface.

The morphology of GQDs and functionalized GQDs was studied by TEM. Fig. 2A indicates that the diameters of the as-prepared GQDs are in the range of 3–10 nm, with an average value of ~8 nm in size. The high resolution TEM (HRTEM) result clearly shows high crystallinity of the GQDs, with a lattice parameter of 0.241 nm, (1 1 2 0) lattice fringes of graphene [8]. Fig. 2B indicates that hemin-functionalized GQDs with the average diameter of 9.5 nm are slightly larger than GQDs.

X-ray photoelectron spectroscopy (XPS) was employed to further explore the interaction between hemin and GQDs. The survey (Fig. 3A) of GQDs showed a C_{1s} peak at 285 eV and an O_{1s} peak at 398 eV. Compared with GQDs, the survey (Fig. 3B) of hemin-functionalized GQDs showed the presence of an N_{1s} peak at 398 eV

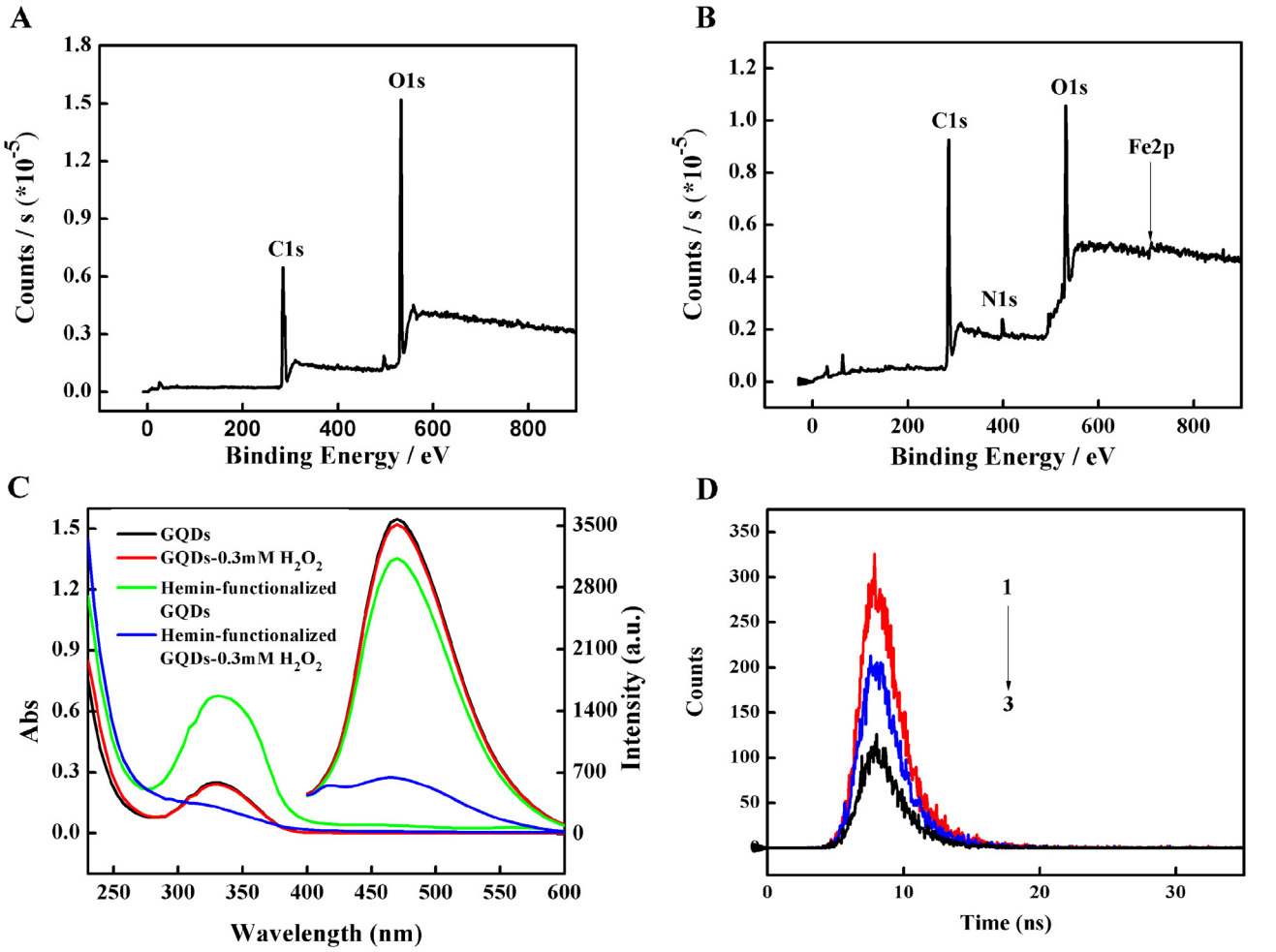

Fig. 3. (A) XPS survey spectrum of GQDs. (B) XPS survey spectrum of hemin-functionalized GQDs. (C) UV and FL spectrum of GQDs and hemin-functionalized GQDs solution in the absence and presence of H_2O_2. (D) The FL decay curves of GQDs in the absence and presence of H_2O_2. 1–3: 0, 10, and 50 μM.

Table 1
The fit results of fluorescence lifetimes before and after quenching of GQDs.

CH_2O_2 (μM)	τ_1 (ns)	τ_2 (ns)	B_1	B_2	χ^2	τ (ns)
0	1	2.7	258.16	104.93	1.017	1.89
10	1	3.7	254.56	35.02	1.010	1.91
50	1	2.8	85.49	38.26	1.025	2.00

and a Fe_{2p} peak at about 711 eV originating from hemin, indicating that the noncovalent functionalization of GQDs by hemin successfully occurred.

3.2. FL response of the GQDs to H_2O_2 and the corresponding mechanism

The feasibility of strategy for H_2O_2 detection based on the FL quenching of hemin-functionalized GQDs was investigated. As shown as Fig. 3C, H_2O_2 has nearly no effect on the FL signal of GQDs, while the hemin-functionalized GQDs were very sensitive to H_2O_2 (Fig. 3C, blue curve), and 0.3 mM H_2O_2 completely quenched the FL of GQDs. The result is in agreement with the literature [10] that indicated some reactive oxygen species except for •OH (such as H_2O_2) have nearly no effect on the FL signal of GQDs.

Although the exact mechanism of carbon-based quantum dots is still an open question, it is now increasingly adopted that radioactive recombination of the carbon nanoparticle surface-confined electrons and holes are responsible for the observed bright FL. The electrons and holes are likely generated by efficient photo induced charge separations in the carbon nanoparticles, and the role of surface passivation is probably to make the surface sites more stable to facilitate more effective radioactive recombination [6]. The GQDs prepared by the incompletely carbonized citric acid are surface-passivated and thus have good fluorescence activity [10]. When hemin was adsorbed on the GQDs' surface to form hemin-functionalized GQDs, the FL intensity decreased a little (with a quenching extent of 9.1%), which could be that the assembly of hemin affected the surface state of GQDs. When mixed with H_2O_2, a sharp drop of FL intensity of hemin-functionalized GQDs was detected (with a quenching extent of 86%). The quenching of bright FL emission is probably due to the destruction of surface passivation of GQDs. Since the contribution from individual H_2O_2 to the FL quenching of the GQDs is negligible, we suppose that free radicals generated from hemin-media reaction led to the FL quenching. In the hemin-catalyzed H_2O_2 reaction, two different types of free radicals, hydroxyl and carbon-centered radicals, were identified [25]. Because of the strong oxidizing nature of these free radicals, the surface passivation of the GQDs could be destroyed. The UV–vis absorption spectroscopy (Fig. 3C) also supported the conclusion. The characteristic absorption of hemin-functionalized GQDs at 372 nm almost disappeared in the presence of 0.3 mM H_2O_2, indicating that the surface passivation of GQDs was destroyed.

To further verify this mechanism, the fluorescence decays were examined (Table 1). Fig. 3D shows the decay curves of GQDs in the absence and presence of H_2O_2. The FL lifetimes changed little with increasing H_2O_2, and the FL quenching was mainly associated with a drop of the initial height of the decay curves, meaning static quenching dominates over dynamic quenching [26,27]. The average lifetime was found to be only 1.93 nm, which reflects a fast exciton recombination process [28,29].

3.3. Optimization of assay conditions

Several experimental parameters were systematically investigated to establish optimal conditions for the proposed fluorescence sensor (Fig. 4), including the concentration of GQDs and hemin, the pH values of the buffer and incubation time.

We optimized the incubation time of the sensing system, and the fluorescence intensity of the system at 470 nm reached a minimum in 10 min (Fig. 4A). Hence, incubation time of 10 min was chosen for subsequent experiments.

The concentration of GQDs was a key factor in this sensing system. The effect of different amounts of GQDs was investigated (Fig. 4B). The experiment results showed that the fluorescence intensity of the system was increasing gradually with the concentration of GQDs. To find the optimum the concentration of GQDs, the relative fluorescence quenching effect $(F_0–F)/F_0$ were compared at different the concentration of GQDs. In order to give attention to both the sensitivity and linear range, 50 μg mL^{-1} GQDs solution was used for the subsequent FL measurements.

The proposed FL probe was pH-dependent due to the –COOH on the surface of the GQDs, so we investigated the effect of pH on the fluorescence intensity of the GQDs sensor system from 5.2 to 8.3 (Fig. 4C). The experimental results showed that the maximal response of the biosensor was obtained at pH 7.0. Thus the optimum pH was achieved for buffer solution at pH 7.0. We investigated the effect of different amounts of hemin on the fluorescence quenching effect. As shown in Fig. 4D, the fluorescence quenching effect firstly increased with increasing amount of hemin and tended to reach a maximum value at 2.5 μM. Therefore, the 2.5 μM hemin was adopted in the subsequent work.

3.4. Analytical performance of the biosensor for H_2O_2 measurements

Under the optimized conditions, response to H_2O_2 concentration was linear in the range from 1 μM to 300 μM with a limit detection of 0.1 μM at three times the standard deviation of the blank response (Fig. 5 A and B).The regression equation is $F_0/F = 0.02C + 0.98$ (Where F_0 and F were the fluorescence intensity of the system at 471 nm in the presence and absence of H_2O_2, and where C was the concentration of H_2O_2, μM) with a correlation coefficient of 0.996. For estimating the precision, a series of eleven repetitive measurements of H_2O_2 yielded reproducible signals with a relative standard deviation of 2.1%.

3.5. Glucose detection with this hemin-functionalized GQDs-based biosensor and glucose oxidase

The proposed biosensor coupling with glucose oxidase as molecular recognition element, make it possible to extend the sensing system for glucose detection (Fig. 5C and D). The calibration curve for glucose detection using hemin-functionalized GQDs and glucose oxidase exhibited a linear range from 9 μM to 300 μM, and the a regression equation was $F_0/F = 0.0095C + 0.86$ (Where F_0 and F were the fluorescence intensity of the system at 471 nm in the presence and absence of glucose, and where C was the concentration of glucose, μM) with a correlation coefficient of 0.99. The limit of detection was 0.1 μM at three times the standard deviation of the blank response. For estimating the precision, a series of eleven repetitive measurements of 50 μM glucose yielded reproducible signals with a relative standard deviation of 3.5%. Moreover, a comparison between the proposed method and other reported methods for glucose determination in detection limit and linear range was summed up in Table 2. It was evident that the sensitivity of the method was better than most of the reported methods.

The selectivity of the proposed biosensor for glucose was evaluated before its application in a real sample. The influence of some biological species including metal ions, amino acids, and proteins (such as BSA) were investigated (Fig. 6). Compared to the response to 50 μM glucose alone, 1000 times of Na^+, K^+, Cl^- and NO_3^-, 100 times of Mg^{2+} and HPO_4^{2-}, 10 times of Ca^{2+}, Zn^{2+} and

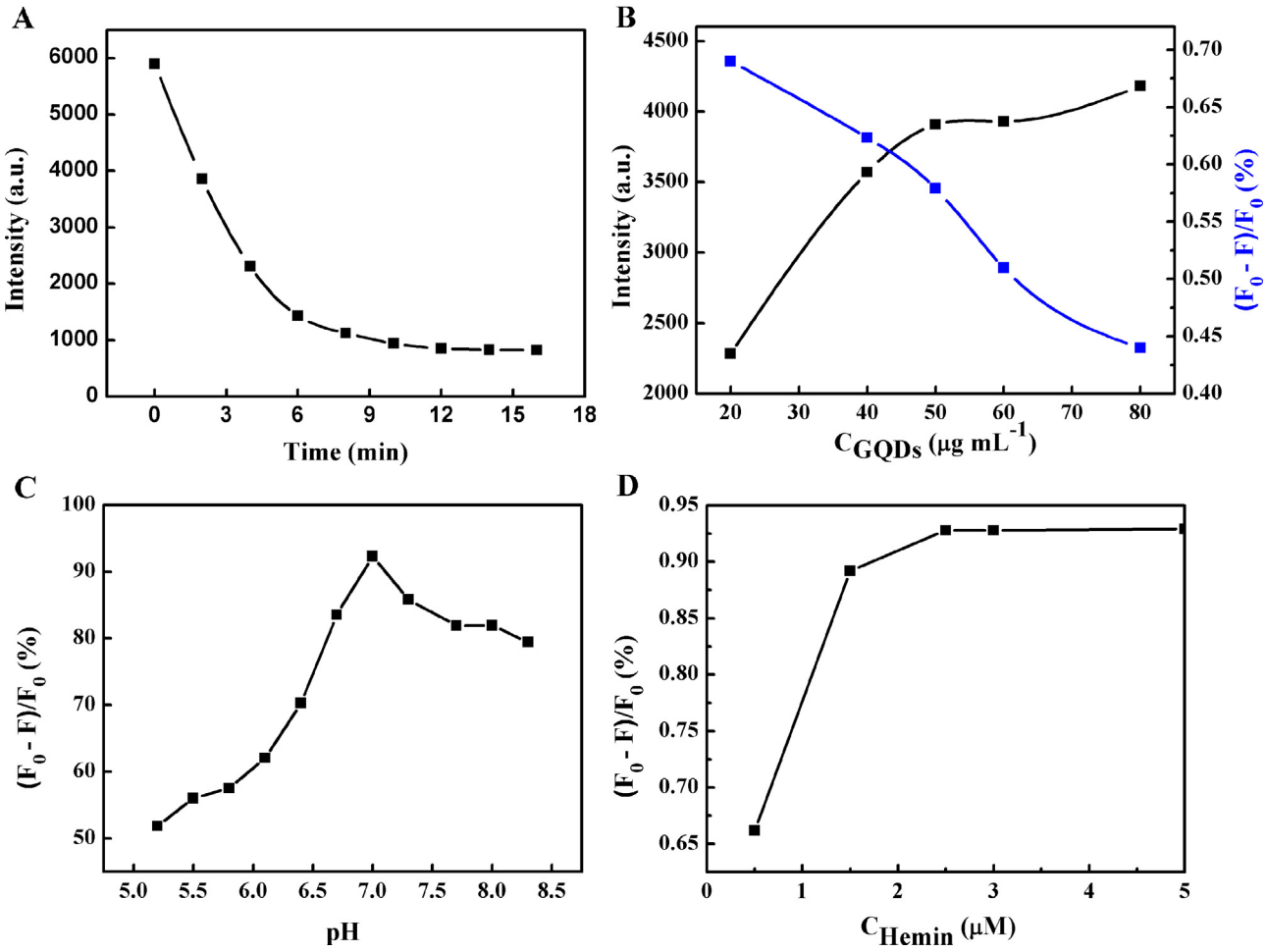

Fig. 4. Effects of (A) incubation time, (B) GQDs concentration, (C) pH, and (D) hemin concentration at the proposed biosensor.

Table 2
Comparison of different methods for glucose detection.

Method	System	Linear range (μM)	LOD (μM)	Ref.
Electrochemistry	Silver nano on Cu rod/GOx	20–7400	0.1	[28]
Colorimetry	C-Dots/GOx/TMB	1–100	0.2	[29]
Electrochemistry	Graphene oxide/GOx	100–1400	–	[30]
Colorimetry	Graphene oxide/GOx/TMB	1–20	1	[31]
Electrochemistry	GQDs/GOx	5–1270	1.73	[32]
Fluorometry	HAQB/GOx	80–420	11	[33]
Electrochemistry	CuO nano/methylene blue	900–1600	20	[34]
Colorimetry	Cu nano/GOx/TMB	100–2000	100	[35]
Electrochemistry	FeSe thin film/GOx	2–30	0.5	[36]
Fluorometry	Hemin-functionalized GQDs/GOx	9–300	0.1	This sensor

Al^{3+} did not interfere the determination of glucose. The same concentrations of uric acid, ascorbic acid, dopamine, BSA and some amino acids such as L-tryptophan, L-tyrosine and did not interfere the determination of glucose. The presence of different foreign species on the biosensor response to glucose was investigated. The tolerable amounts of interfering species were added. The results clearly demonstrated the specificity of the sensing system for glucose.

Table 3
Analysis of glucose in serum samples.

Serum samples	Measured (mM)		Added glucose (μM)	Recovery (%)	RSD% ($n = 3$)
	The proposed sensor[a]	Hospital			
1	5.98	6.39	50	107.2	2.64
2	4.97	5.89	50	97.6	1.52
3	7.64	8.20	50	103.9	1.00
4	5.31	5.56	50	98.9	4.50

[a] Serum samples were diluted 100-folds.

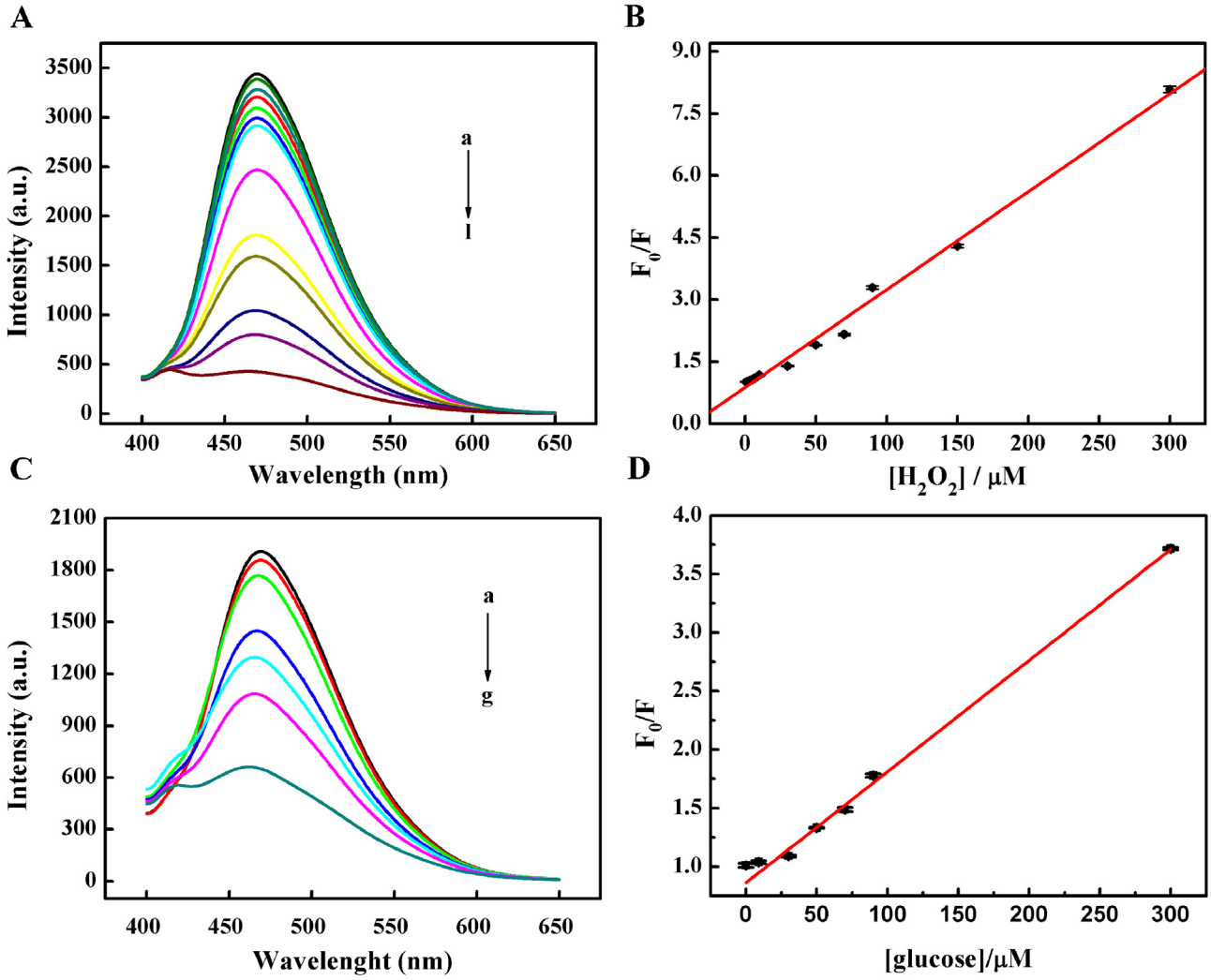

Fig. 5. (A) FL emission spectra of the sensing system after addition of various amounts of H_2O_2 (a–l: 0, 1, 3, 5, 7, 9, 10, 30, 50, 70, 90, 150, and 300 μM). (B) The relationship between the florescence quenching and the concentration of H_2O_2. (C) FL emission spectra of the sensing system after addition of various amounts of glucose (a–g: 0, 9, 30, 50, 70, 90, and 300 μM). (D) The relationship between the florescence quenching and the concentration of glucose.

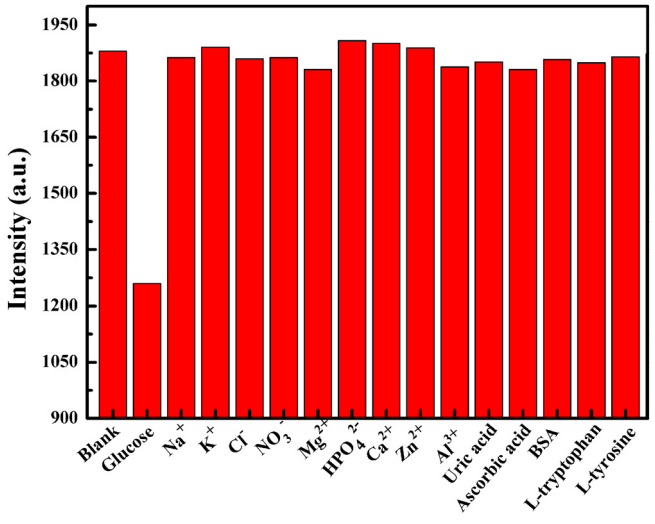

Fig. 6. The FL response of the sensing system in the presence of 50 μM glucose; 50 mM Na^+, K^+, Cl^-, and NO_3^-; 5 mM Mg^{2+} and HPO_4^{2-}; 0.5 mM Ca^{2+}, Zn^{2+}, and Al^{3+}; 50 μM uric acid, ascorbic acid, dopamine, BSA, L-tryptophan, and L-tyrosine.

3.6. Analytical applications in real serum sample

Serum samples were provided by Anhui Normal University Hospital. The fresh serum samples were analyzed by the proposed method and the spectrophotometric test which was performed by Anhui Normal University Hospital. As shown in Table 3, the values measured by the developed biosensor were in good agreement with the results from the standard spectrophotometric method. The recoveries of the samples were found to be in the range of 97.6% to 107.2% with the RSD within 5.0%, which indicated the proposed method was reliable for detecting glucose in biological samples.

4. Conclusion

In summary, the hemin-functionalized GQDs were firstly used as FL sensing platform for the detection of H_2O_2 and glucose. The as-prepared GQDs which were surface-passivated have good fluorescence activity and favorable biocompatibility. Through electrostatic and π–π stacking interaction, hemin was introduced via simple adsorption on GQDs to form hemin/GQDs nanocomposites. With the aid of hemin, H_2O_2 could destroy the passivated surface of GQDs and quench the FL signal obviously. Based on this effect, we designed a label-free fluorescence biosensor to detect glucose

in human serum samples. Furthermore, the eco-friendly, cost-efficient and simple hemin-functionalized GQDs-based biosensor showed great promising applications in the clinical diagnosis and medicine.

Acknowledgments

This work was supported by Natural Science Foundation of China (21075002, 21275008, and 21245008).

References

[1] S.J. Rosenthal, J.C. Chang, O. Kovtun, J.R. McBride, I.D. Tomlinson, Chem. Biol. 18 (2011) 10–24.
[2] M. Bruchez Jr., Science 281 (1998) 2013–2016.
[3] A. Valizadeh, H. Mikaeili, M. Samiei, S. Farkhani, N. Zarghami, M. kouhi, A. Akbarzadeh, S. Davaran, Nanoscale Res. Lett. 7 (2012) 1–14.
[4] L. Cao, X. Wang, M.J. Meziani, F. Lu, H. Wang, P.G. Luo, Y. Lin, B.A. Harruff, L.M. Veca, D. Murray, S.Y. Xie, Y.P. Sun, J. Am. Chem. Soc. 129 (2007) 11318–11319.
[5] Z. Zhang, J. Zhang, N. Chen, L. Qu, Energ. Environ. Sci. 5 (2012) 8869–8890.
[6] L. Cao, M.J. Meziani, S. Sahu, Y.P. Sun, Acc. Chem. Res. (2012) 171–180.
[7] L.A. Ponomarenko, F. Schedin, M.I. Katsnelson, R. Yang, E.W. Hill, K.S. Novoselov, A.K. Geim, Science 320 (2008) 356–358.
[8] J. Peng, W. Gao, B.K. Gupta, Z. Liu, R. Romero-Aburto, L. Ge, L. Song, L.B. Alemany, X. Zhan, G. Gao, S.A. Vithayathil, B.A. Kaipparettu, A.A. Marti, T. Hayashi, J.J. Zhu, P.M. Ajayan, Nano Lett. 12 (2012) 844–849.
[9] S.J. Zhu, J.H. Zhang, C.Y. Qiao, S.J. Tang, Y.F. Li, W.J. Yuan, B. Li, L. Tian, F. Liu, R. Hu, H.N. Gao, H.T. Wei, H. Zhang, H.C. Sun, B. Yang, Chem. Commun. 47 (2011) 6858–6860.
[10] Y. Dong, G. Li, N. Zhou, R. Wang, Y. Chi, G. Chen, Anal. Chem. 84 (2012) 8378–8382.
[11] J.J. Liu, X.L. Zhang, Z.X. Cong, Z.T. Chen, H.-H. Yang, G.N. Chen, Nanoscale 5 (2013) 1810–1815.
[12] J. Shen, Y. Zhu, X. Yang, C. Li, Chem. Commun. 48 (2012) 3686–3688.
[13] V. Georgakilas, M. Otyepka, A.B. Bourlinos, V. Chandra, N. Kim, K.C. Kemp, P. Hobza, R. Zboril, K.S. Kim, Chem. Rev. 112 (2012) 6156–6214.
[14] Y. Xu, Z. Liu, X. Zhang, Y. Wang, J. Tian, Y. Huang, Y. Ma, X. Zhang, Y. Chen, Adv. Mater. 21 (2009) 1275–1279.
[15] T. Xue, S. Jiang, Y. Qu, Q. Su, R. Cheng, S. Dubin, C.Y. Chiu, R. Kaner, Y. Huang, X. Duan, Angew. Chem. 124 (2012) 3888–3891.
[16] Y. Xu, L. Zhao, H. Bai, W. Hong, C. Li, G. Shi, J. Am. Chem. Soc. 131 (2009) 13490–13497.
[17] Y. Song, W. Wei, X. Qu, Adv. Mater. 23 (2011) 4215–4236.
[18] Y. Guo, L. Deng, J. Li, S. Guo, E. Wang, S. Dong, ACS Nano 5 (2011) 1282–1290.
[19] L. Wu, J. Wang, L. Feng, J. Ren, W. Wei, X. Qu, Adv. Mater. 24 (2012) 2447–2452.
[20] W. Tu, J. Lei, S. Zhang, H. Ju, Chem.—Eur. J. 16 (2010) 10771–10777.
[21] Y. Song, Y. Chen, L. Feng, J. Ren, X. Qu, Chem. Commun. 47 (2011) 4436–4438.
[22] Y. Dong, J. Shao, C. Chen, H. Li, R. Wang, Y. Chi, X. Lin, G. Chen, Carbon 50 (2012) 4738–4743.
[25] J. Ostermann, J.-P. Merkl, S. Flessau, C. Wolter, A. Kornowksi, C. Schmidtke, A. Pietsch, H. Kloust, A. Feld, H. Weller, ACS Nano (2013), 10.1021/nn4037859.
[26] S.N. Baker, G.A. Baker, Angew. Chem. Int. Ed. 49 (2010) 6726–6744.
[27] S. Mitra, S. Chandra, S.H. Pathan, N. Sikdar, P. Pramanik, A. Goswami, RSC Adv. 3 (2013) 3189–3193.
[28] X.J. Zhang, R. Ji, L.L. Wang, L.T. Yu, J. Wang, B.Y. Geng, G.F. Wang, CrystEngComm 15 (2013) 1173–1178.
[29] W.B. Shi, Q.L. Wang, Y.J. Long, Z.L. Cheng, S.H. Chen, H.Z. Zheng, Y.M. Huang, Chem. Commun. 47 (2011) 6695–6697.
[30] H.W. Yang, M.Y. Hua, S.L. Chen, R.Y. Tsai, Biosens. Bioelectron. 41 (2013) 172–179.
[31] Y. Song, K. Qu, C. Zhao, J. Ren, X. Qu, Adv. Mater. 22 (2010) 2206–2210.
[32] H. Razmi, R. Mohammad-Rezaei, Biosens. Bioelectron. 41 (2013) 498–504.
[33] K. Wannajuk, M. Jamkatoke, T. Tuntulani, B. Tomapatanaget, Tetrahedron 68 (2012) 8899–8904.
[34] M.U.A. Prathap, B. Kaur, R. Srivastava, J. Colloid Interface Sci. 370 (2012) 144–154.
[35] L. Hu, Y. Yuan, L. Zhang, J. Zhao, S. Majeed, G. Xu, Anal. Chim. Acta 762 (2013) 83–86.
[36] A.K. Dutta, S.K. Maji, A. Mondal, B. Karmakar, P. Biswas, B. Adhikary, Sens. Actuators, B 173 (2012) 724–734.